Original Research *Highlight article*

Establishment of a mouse model for ovarian cancer–associated venous thromboembolism

Sining Ma[1,2*], Sheng Yin[1,2*], Yiyan Zheng[1] and Rongyu Zang[1]

[1]Ovarian Cancer Program, Department of Gynecologic Oncology, Zhongshan Hospital, Fudan University, Shanghai 200032, China;
[2]Department of Obstetrics and Gynecology, Zhongshan Hospital, Fudan University, Shanghai 200032, China
*These authors contributed equally to this paper.
Corresponding authors: Yiyan Zheng. Email: yiyanzheng@fudan.edu.cn; Rongyu Zang. Email: zang.rongyu@zs-hospital.sh.cn

Impact Statement

An animal model is beneficial for investigating the physiological and pathological processes in ovarian cancer–associated venous thromboembolism (OC-VTE). To our knowledge, however, there has not been any report about an animal model of OC-VTE. In this study, we generated a mouse model of OC-VTE using inferior vena cava (IVC) stenosis combined with inoculating the ovarian cancer cell line into severe combined immunodeficiency disease (SCID) mice. Our study represents an attractive future research direction and lays the foundation for unraveling the underlying molecular mechanisms of OC-VTE formation.

Abstract

Patients with ovarian cancer are at increased risk of venous thromboembolism (VTE), and the cumulative incidence is high, particularly at advanced stages of this disease. Nevertheless, it is challenging to investigate the molecular mechanisms of ovarian cancer–associated VTE (OC-VTE), mainly due to the lack of a well-developed animal model for this disease. We generated a mouse model for developing OC-VTE using ovarian cancer cell injection in combination with the inferior vena cava stenosis method. The rate of thrombosis in the OC-VTE group was 50%, compared with 0 in the control group. Moreover, we conducted a proteomic analysis using platelets from these models and revealed differentially expressed proteins between the OC-VTE and control groups, including upregulated and downregulated proteins. Gene Ontology analysis revealed that these differentially expressed proteins were mostly enriched in the biological process of negative regulation of fibrinolysis and the cellular component of the fibrinogen complex, both of which play key roles in thrombosis. In conclusion, this study lays the foundation for further investigation of the underlying mechanisms of how ovarian cancer promotes VTE formation.

Keywords: Venous thromboembolism, ovarian cancer, mouse model, platelet, inferior vena cava stenosis, proteomic analysis

***Experimental Biology and Medicine* 2022; 248: 26–35. DOI: 10.1177/15353702221118533**

Introduction

Cancer patients are at increased risk of developing venous thromboembolism (VTE), including deep vein thrombosis (DVT) and pulmonary embolism (PE).[1–4] Patients with cancer and VTE have a poor prognosis.[5] Indeed, patients with cancer who develop VTE have an increased risk of recurrent thrombosis and a two- to sixfold increase in mortality compared with patients without cancer. VTE is the second most common cause of death in cancer patients.[1,6] The number of hospitalized cancer patients with VTE has been on the rise over the last few decades, with a prevalence of 2–7.3%.[7] VTE is observed in 5.2% of cancer patients with solid tumors and VTE rates are the highest among pancreatic and ovarian cancer patients.[8]

The two-year cumulative incidence of VTE in patients with ovarian cancer is around 7.2% and the cumulative incidence is higher at the advanced stages of the disease.[9] In Asia, ovarian cancer patients are at a high risk of developing VTE.[10] In addition, silent VTE is frequently identified in patients with ovarian cancer before receiving clinical treatment.[10] Therefore, it is vital to unravel the underlying mechanisms of how malignancy contributes to VTE development in patients with ovarian cancer, which might help lay the foundation for developing therapeutic strategies for these patients.

Different risk factors contributing to VTE have been identified in clinics, but the detailed mechanisms underlying thrombus initiation and development are not completely understood. A thrombus comprises red blood cells, fibrin, and platelets.[11] Activated platelets serve as a binding surface for tissue factor (TF) recruitment, necessary for the thrombotic process.[12] Platelet recruitment mediated by von Willebrand Factor (VWF) to the vascular wall also plays a critical role in initiating venous thrombosis.[13] Still, whether the platelets play the same role in cancer-associated VTE remains incompletely understood. The underlying mechanisms of how cancer-associated VTE initiates and develops remain elusive. Performing molecular analyses of cancer-associated VTE can be challenging for two main reasons: tumor heterogeneity (potentially leading to cancer type–specific mechanisms of

ISSN 1535-3702

VTE) and the lack of a well-developed animal model for this condition. Therefore, the generation of a specific animal model is a key to investigating the initiation and development of cancer-associated VTE.

The mouse model is amenable, making it ideal for studying venous thrombosis, with the advantage of choosing between different strains and being cost-efficient. Technically, the optimal VTE mouse model should be easy to produce and induce thrombus formation in the veins with identical thrombus size.[14] Spontaneous development of VTE in mice is highly unlikely; therefore, researchers employ various approaches to trigger and accelerate thrombosis within veins, including ferric chloride ($FeCl_3$) presoaking,[15] jugular vein injection,[16] inferior vena cava (IVC) ligation model,[17] and IVC stenosis.[18]

The ferric chloride model involves placing a filter paper soaked with $FeCl_3$ solution on the surface of a vein for a limited time. This causes transmural injury to the vessel and results in occlusive thrombosis.[15] An injection of a mixture of collagen and epinephrine into the jugular vein induces platelet aggregation, leading to acute thrombosis.[16] These models mimic acute thrombosis and therefore are only representative of a small part of clinical VTEs. They are not characteristic of VTE induced by tumors, which tend to be chronic.[19] The other two thrombosis models, IVC ligation and IVC stenosis, have been reported to induce chronic venous thrombosis.[20,21] Nevertheless, IVC ligation induces injury to the endothelium of the vein wall, leading to thrombi formation and making it nonideal to model the process of cancer-associated venous thrombosis. In contrast, IVC stenosis does not impair the integrity of the vein endothelium layer, which is more suitable for modeling venous thrombosis induced by cancer cells. A 90% IVC stenosis strategy (reducing lumen size by around 90%) has been used to induce thrombosis in a mouse model of pancreatic cancer, but it leads to acute venous thrombi formation due to excessive IVC stenosis.[22] Thus, how to generate a mouse model with a chronic formation of cancer-associated VTE remains a challenge.

In this study, we generated an OC-VTE mouse model using the ovarian cancer cell injection strategy in combination with 50% IVC stenosis (reducing IVC lumen size by around 50%). In addition, we performed a proteomic analysis using platelets from this mouse model and revealed proteins potentially involved in the formation of OC-VTE.

Materials and methods

Animals

Severe combined immunodeficiency disease (SCID) mice aged four to six weeks, with an average body weight of 16 g, were used in this study. One hundred two mice were randomly selected to receive an intraperitoneal graft of SKOV3 cells combined with 50% IVC stenosis to induce a thrombus (OC-VTE model group) and survived five days after modeling. Fifteen mice were used as the control group and received IVC stenosis only.

All animal experiments in this study were conducted in accordance with the Institutional Animal Care and Use Committee (IACUC) standards and guidelines. All experiments were approved by the animal research committee of Zhongshan Hospital of Fudan University. According to the procedure approved by Zhongshan Hospital of Fudan University, all mice were ultimately sacrificed by cervical dislocation after carbon dioxide exposure.

Establishment of the OC-VTE mouse model

Establishment of intraperitoneal tumor model. The human ovarian serous adenocarcinoma cell line SKOV3 was cultured in RPMI-1640 medium supplemented with 10% fetal bovine serum, 50 U/mL penicillin-streptomycin, and incubated in 5% CO_2 at 37°C. Each mouse in the OC-VTE group was intraperitoneally injected with 1×10^7 SKOV3 cells. Briefly, the abdominal skin was cleaned and disinfected, and an intraperitoneal injection of 200 µL of PBS with SKOV3 cells was performed using a needle in the left hypochondrium quadrant of the abdomen. Abdominal tumor formation and animal survival were assessed from injection to day 21 and body weight was checked weekly. On days 7, 14, and 21 after intraperitoneal injection, all surviving mice for the experiment underwent laparotomy for tumor evaluation. The model's optimum status was identified once the macroscopic tumor nodules were formed and allowed for a relatively long-time survival.

Infrarenal IVC stenosis procedure. Once the macroscopic tumor nodules formed, all the surviving mice would receive surgery for IVC stenosis. Briefly, the mice were anesthetized with an intraperitoneal injection of 0.3% pentobarbital sodium 0.1 mL and placed supine. After laparotomy and gently dissecting the IVC from the aorta, the IVC was ligated on a 20-gauge (R = 0.45 mm), 22-gauge (R = 0.35 mm), and 26-gauge needle (R = 0.23 mm) and the needle was removed for partial blood flow restriction (stenosis), causing 20%, 50%, and 80% stenosis, respectively (calculated as area = $(1 - \pi R_{needle}^2 / \pi R_{IVC}^2) \times 100\%$, and R_{IVC} was supposed as 0.5 mm, according to our experiments). The needle was positioned outside the vessel to avoid puncture or other damage to the IVC wall. All collateral branches were left not ligated. The peritoneum and skin were sutured with absorbable monofilament sutures and 6.0 silk sutures, respectively. The best stenosis model was chosen according to a low mortality rate and high VTE rate. All procedures were performed by the same experienced laboratory animal technician.

Model evaluation

The mice that survived more than five days after the IVC procedure and could be observed for VTE formation were considered qualified models. The VTE formation was confirmed by high-frequency ultrasound (HFUS) and histological methods.

HFUS imaging. Ultrasound imaging was performed for each mouse from both experimental and control groups on days 1, 3, 5, and 7 after ligation. IVC thrombosis and blood flow images were monitored by HFUS using a VIVO 2100 ultrasound scanner and a 24.0 MHz linear array transducer (Visual Sonics, Toronto, Canada).

Histological examination. After thrombus formation was observed, a 0.5 cm specimen of the vessel was taken from the proximal and distal ends of the ligated section of the IVC, fixed overnight with 4% neutral formaldehyde, dehydrated with xylene and ethanol, and embedded in paraffin. The transverse sections were 4 µm thick and hematoxylin/eosin staining was performed every 300 µm.

Protein extraction of the platelets

Blood from the right ventricle of the mice was collected with a 1 mL syringe and was immediately transferred into a 10% ethylenediaminetetraacetic acid (EDTA) anticoagulant tube. The tube was left at room temperature for 30 min. An equal volume of PBS was used to dilute the blood sample. The Ficoll-Paque PLUS separation solution (Cytiva, Washington, D.C., USA) (3–5 mL) was added to the bottom of a centrifuge tube. The diluted blood was spread to the top of the separation liquid and centrifuged at 900 rpm for 30 min. The supernatant was transferred to a new centrifuge tube, and five volumes of Hanks solution were added to the tube and centrifuged at 3200 rpm for 20 min. The supernatant was discarded and the platelets were resuspended with 1000 µL of Hanks solution and counted using a blood cell analyzer.

High-performance liquid chromatography-mass spectrometry

The platelets were lysed with 0.1% Rapigest lysate and ultrasound; the ultrasonic pulse intensity was 65%, the pulse intensity was 5 s, the interval was 5 s, and the lysis time was 3 min. The supernatant was taken for protein quantification by the bicinchoninic acid assay (BCA) method. After quantification, the samples were stored at −80°C for later mass spectrometry analysis.

The samples were first digested using trypsin in 50 mM ammonium bicarbonate buffer at 37°C for 16–18 h. The peptides were desalted prior to sample injections. Eluents A and B were 0.1% formic acid aqueous solution and 0.1% formic acid 80% acetonitrile aqueous solution, respectively. The chromatographic column was balanced with 95% A solution. The samples were loaded by an automatic sampler. The gradient elution conditions were as follows: at 0, 50, and 55 min, the linear gradient of eluent B was 0, 35%, and 100%. At 55–60 s, 100% of eluent B was maintained. The mass spectrometric analysis was performed with the Exploris 480 mass spectrometer (Thermo Fisher Scientific, Waltham, MA, USA). A mass spectrometric replicate was performed for each sample to screen for potential intergroup differential proteins by label-free quantitative proteomics. The Thermo Proteome Discoverer 2.4.0.305 software was used to carry out label-free protein identification and quantitative analysis on the original mass spectrum data files. A twofold change was required to consider significance for the proteomic analysis.

ELISA

ELISA was performed to measure the levels of platelet clotting proteins in plasma using an ELISA kit (Boster Biological Technology, Pleasanton, CA, USA). The antibody was diluted with carbonate coating buffer to a protein content of 1–10 µg/mL, and 100 µL was added to each well of a polystyrene microtiter plate at 4°C overnight. The solution was discarded and washed with washing buffer three times, 3 min each time. The wells were blocked using 200 µL of blocking solution to each well and incubated at 37°C for 1–2 h. The sealing film was carefully removed and the plate was washed in a plate washer three to five times. The appropriately diluted samples (100 µL) were added to the wells and incubated at 37°C for 1–2 h. Washing was done as above. The diluted biotinylated antibody working solution (100 µL) was added to each well and incubated at 37°C for 1 h. The plate was washed as above. The enzyme conjugate (100 µL) was added and incubated at 37°C in the dark for 30 min. The plate was washed as above. The TMB chromogenic substrate (100 µL) was added to each well and incubated for 10–30 min at 37°C in the dark until a clear color gradient appeared in the standard curve wells. The reaction was terminated with 100 µL of 2 M sulfuric acid. Within 10 min, the optical density (OD) value of each well was measured after zeroing the blank control well at 450 nm on a microplate reader.

Results

Generation of OC-VTE mouse model

First, we set out to generate a cell line–derived xenograft mouse model for ovarian cancer using the SKOV3 cell line. The results indicated that day 14 post-tumor engraftment was the ideal time point for carrying out IVC stenosis operation when mice presented with moderate tumor nodules that were not fatal (Figure 1(A)). Next, three models of IVC stenosis (20%, 50%, and 80%) were set up to optimize the stenosis strategy to generate the OC-VTE mouse model. The data showed that 20% of IVC stenosis failed to induce VTE, while 80% of IVC stenosis resulted in a high mortality rate of mice with ovarian cancer tumors. On the contrary, 50% IVC stenosis induced VTE in tumor-bearing mice without highly affecting their mortality rate (Figure 1(B)). Thus, 50% IVC stenosis was selected for VTE mouse model generation. For model evaluation, most formed thrombus could be observed on the postoperative day 3 by HFUS and then stabilized, and postoperative day 5 was chosen to evaluate VTE formation (Figure 1(C)). The details of the IVC stenosis surgical procedure are shown in Figure 2.

Evaluation of thrombosis in the OC-VTE mouse model

Since the density of a thrombus is higher than that of surrounding adipose tissue, the presence of an IVC thrombus could be documented using ultrasound. Thus, ultrasound imaging was selected to examine the blood flow of mouse IVC and investigate the thrombosis in the mice with 50% IVC stenosis in the presence or absence of ovarian cancer tumor burden. In this study, we used HFUS with the color Doppler to examine the direction of blood flow in the mouse IVC. For the mice in the control group, the blood vessel downstream from the stenosis site was narrower 5 days after the 50% IVC stenosis operation. There was no thrombus formation in the blood vessel upstream of the stenosis site, as shown in the representative pictures in Figure 3(A). Color

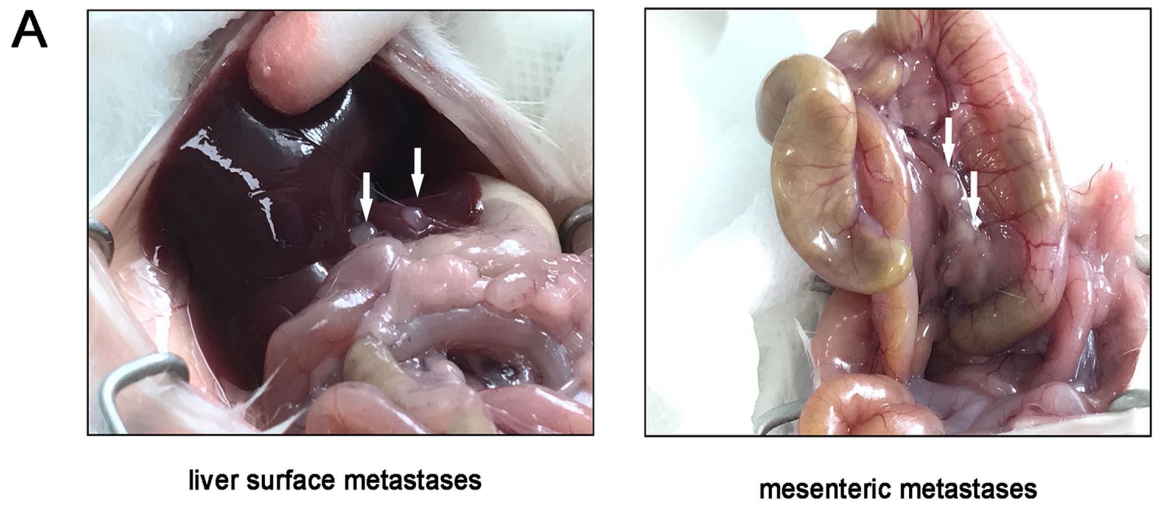

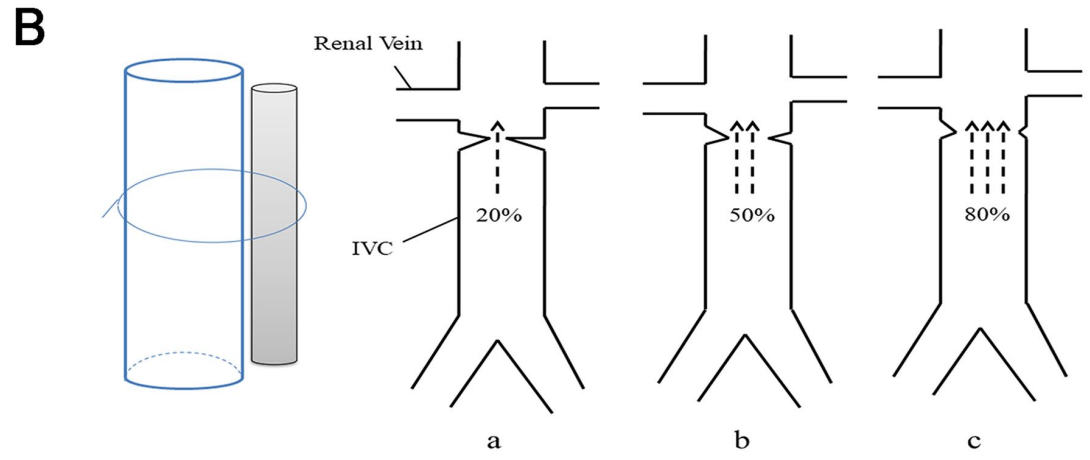

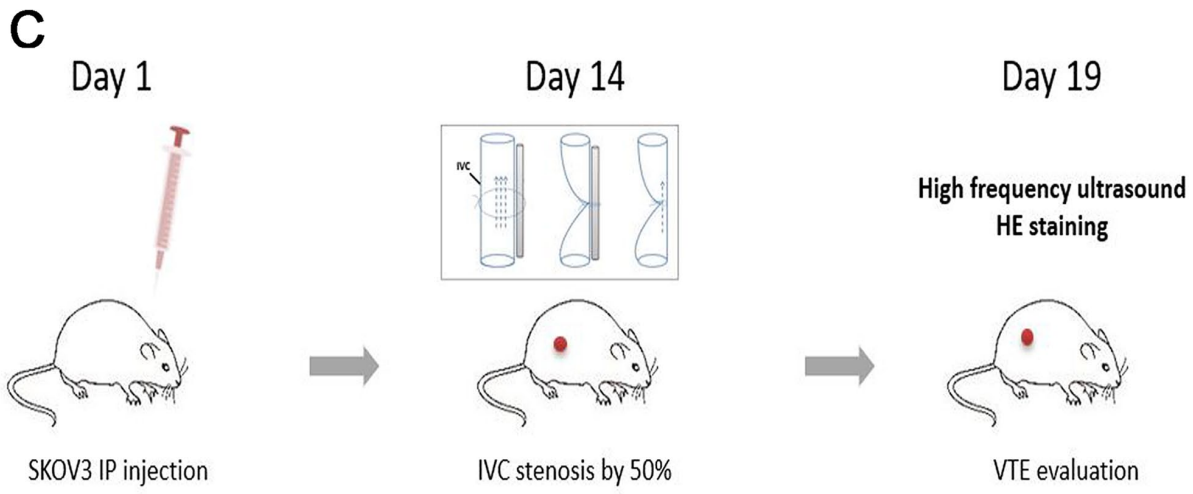

Figure 1. Experimental strategy. (A) Intraperitoneal tumor model was established by SKOV3 injection on day 1, and the optimum status of the model was identified once the macroscopic tumor nodules formed. According to our experiment, appropriate 8–10 tumor nodules were macroscopic on day 14 after SKOV3 injection, allowing a relatively long-time survival, and the following IVC stenosis experiment could be performed. (B) On day 14, once the macroscopic tumor nodules formed, all the surviving mice underwent surgery for IVC stenosis. Three models of IVC stenosis (20%, 50%, and 80%) were set up to optimize the stenosis strategy to generate the ovarian cancer–associated VTE mouse model (the best model of IVC stenosis was chosen in which a low mortality rate and high VTE rate were observed). (C) The whole procedures for generating ovarian cancer–associated VTE models are shown in the cartoons. Ultrasound and H&E staining were used to evaluate thrombosis.

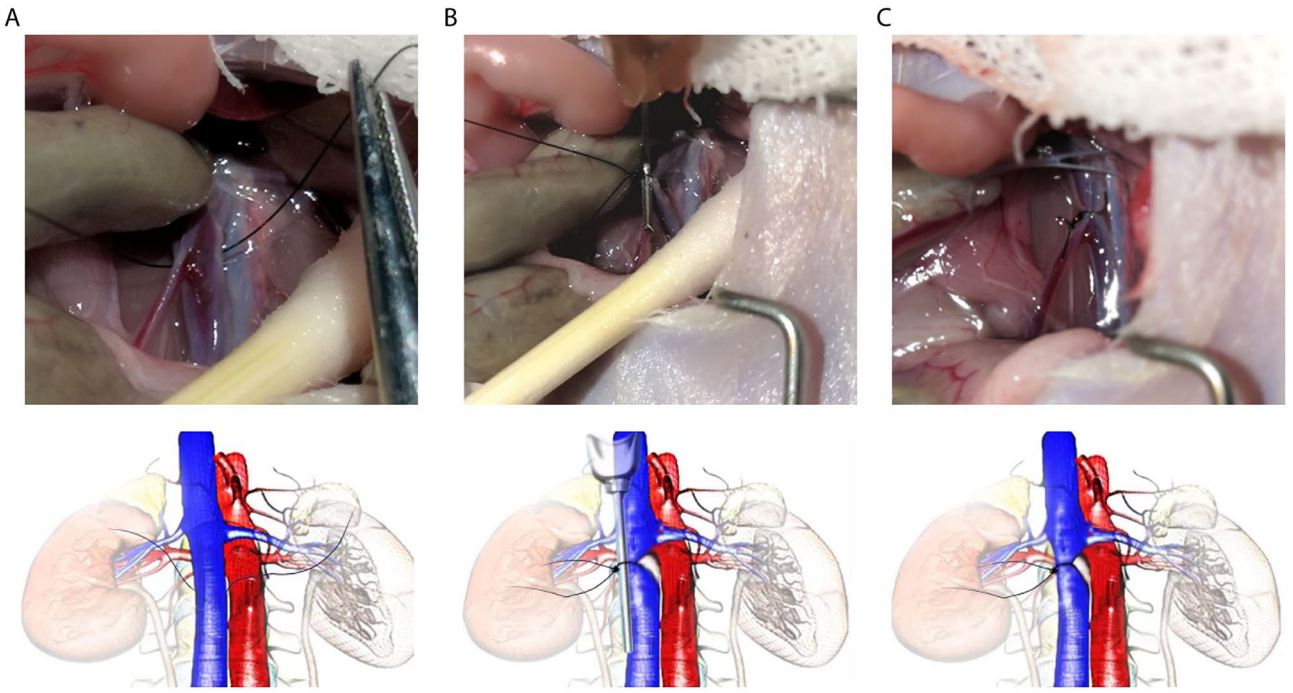

Figure 2. Surgical illustrations for inferior vena cava (IVC) stenosis. (A) The silk thread passed through the back of the inferior vena cava, below the renal vein but above the reproductive vein. The surgical cartoon is shown on the bottom panel for further illustration. (B) The 22-gauge needle was positioned outside the blood vessel to avoid damaging the capillary endothelium and was fastened. The surgical cartoon is shown on the bottom panel for further illustration. (C) The needle was gently removed to reduce 50% of the blood vessel diameter (measured with a caliper, calculated area = πR^2). During the operation, all collateral branches were not ligated. The surgical cartoon is shown on the bottom panel for further illustration.

Doppler ultrasound revealed that the blood flow was unobstructed, passing through the stenosis site, further indicating no thrombus in the blood vessel of the mouse from the control group (Figure 3(A), right panel). In contrast, there was striking thrombus formation in the blood vessel upstream of the stenosis site in the mouse from the OC-VTE group, as shown in Figure 3(B). Importantly, the vein blood flow was obstructed in the mouse from this group (Figure 3(B), right panel) compared with the one from the control group.

Next, H&E staining was performed using sections of 1 cm vessels with IVC ligation sites in the middle of these 1 cm vessels. As shown in Figure 3(C) and (D), the thrombus ultrastructure was detected in a mouse from the OC-VTE group (ovarian cancer cell injection plus 50% IVC stenosis). The thrombus was multilayered with a mix of platelets and red blood cells in both its head and tail and red blood cells aggregation in the middle, altogether forming a tight polymeric fibrin net. However, the mouse from the control group, with 50% IVC stenosis but without ovarian cancer xenograft, had a smooth venal lumen structure and no thrombosis. Taken together, these data showed that we succeeded in generating an OC-VTE mouse model that can be used for further biological analysis of OC-VTE.

The rate of thrombosis in the OC-VTE mouse model

In total, 117 SCID mice were randomized to the intraperitoneal graft of SKOV3 cells combined with 50% IVC stenosis (OC-VTE model group; $n = 102$) or 50% IVC stenosis only (control group; $n = 15$). Through improvement of surgical practice technique and anesthesia resuscitation, the rate of thrombosis was ultimately increased from 18.2% (first time) to 50% (third time) in the OC-VTE group, as opposed to 0 in the control group (Table 1). The mortality rates at the first time of VTE modeling were 31.3% and 6.7% in the OC-VTE and control groups, respectively. However, the mortality rate was ultimately reduced to 0 in the OC-VTE group at the third time of VTE modeling after surgical practice optimization (Table 1).

Platelet proteomics profiling revealed that most of the differentially expressed proteins from the OC-VTE mouse are enriched in the biological process of negative regulation of fibrinolysis

Given that the platelet is one of the key regulators of thrombosis, we hypothesized that the protein profiling signature of platelets would likely determine their biology and contribution to OC-VTE. Platelets were collected from mice of the control and OC-VTE groups and then lysed for further proteomics analysis using liquid chromatography-tandem mass spectrometry. The experiment identified 115,679 spectra for the control group and 100,840 spectra for the OC-VTE group, corresponding to 2254 proteins in total. Further protein profiling characterized the differentially expressed proteins, including upregulated and downregulated proteins in the OC-VTE group, compared with the control group (Figure 4(A); the top 20 upregulated and 20 downregulated protein names are listed in Figure 4(C)). Next, we performed a Gene Ontology enrichment analysis and revealed that these differentially expressed proteins were mostly enriched in the biological process of negative regulation of fibrinolysis as well as the cellular component of the fibrinogen complex, both

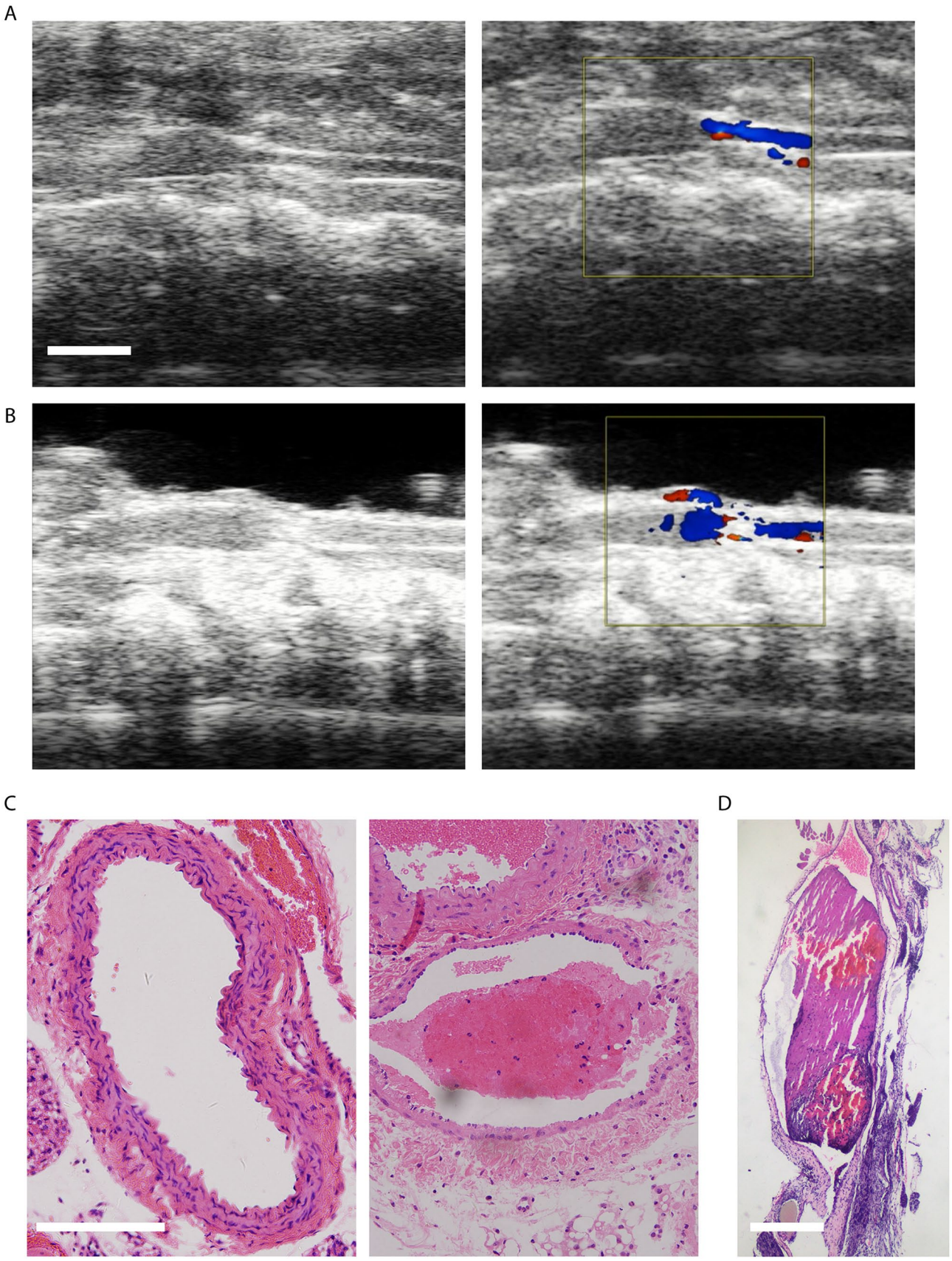

Figure 3. Validation of venous thromboembolism (VTE). (A) After five days of IVC stenosis surgery, a high-frequency ultrasound examination was used to check whether VTE was developed in the control group. The data indicated no thrombus and no blood flow disturbance in the vein. Blue, blood flow in the vein; red, blood flow in the artery. (B) After five days of post-IVC stenosis surgery, a high-frequency ultrasound examination was used to check whether VTE was developed in the OC-VTE group. The data indicated thrombus formation and blood disturbance in the vein. Blue, blood flow in the vein; red, blood flow in the artery. (C and D) H&E staining for the vein sections from the control group (C, left panel) or OC-VTE group (C, right panel; D). Scale bar, 1 mm in C and D.

Table 1. Details of survival and thrombosis of mice in the OC-VTE or control groups.

	Control (15 mice)	OC-VTE-1 (32 mice)	OC-VTE-2 (10 mice)	OC-VTE-3 (60 mice)
Qualified rate	0 (0/15)	12.5% (4/32)	30% (3/10)	50% (30/60)
Mortality rate	6.7% (1/15)	31.3% (10/32)	20% (2/10)	0 (0/60)
Thrombosis rate	0 (0/15)	18.2% (4/22)	37.5% (3/8)	50% (30/60)
Number of deaths	1	10	2	0 (e)
Deaths within POD 2	0	9 (a)	1 (c)	0
Deaths after POD 2	1	1 (b)	1 (d)	0
Number of surviving mice	14	22	8	60
Number of mice with thrombus formation	0	4	3	30

Qualified rate: (number of mice with VTE formation / number of all mice) × 100%; mortality rate: (number of dead mice / number of all mice) × 100%; thrombosis rate: (number of mice with VTE formation / number of surviving mice) × 100%; OC-VTE: ovarian cancer–associated venous thromboembolism; POD: post-operative day. (a), indicating that nine mice died within 2 days after IVC stenosis surgery, including one died of anesthesia accident during IVC stenosis operation, and the other eight died of IVC rupture bleeding during operation. (b), indicating that one mouse died of liver infection disease 2 days after IVC surgery. (c), indicating that one mouse died of anesthesia accident during IVC stenosis operation. (d), indicating that one mouse died on the third day after IVC stenosis surgery. (e), indicating that there was no mouse death in OC-VTE-3 group.

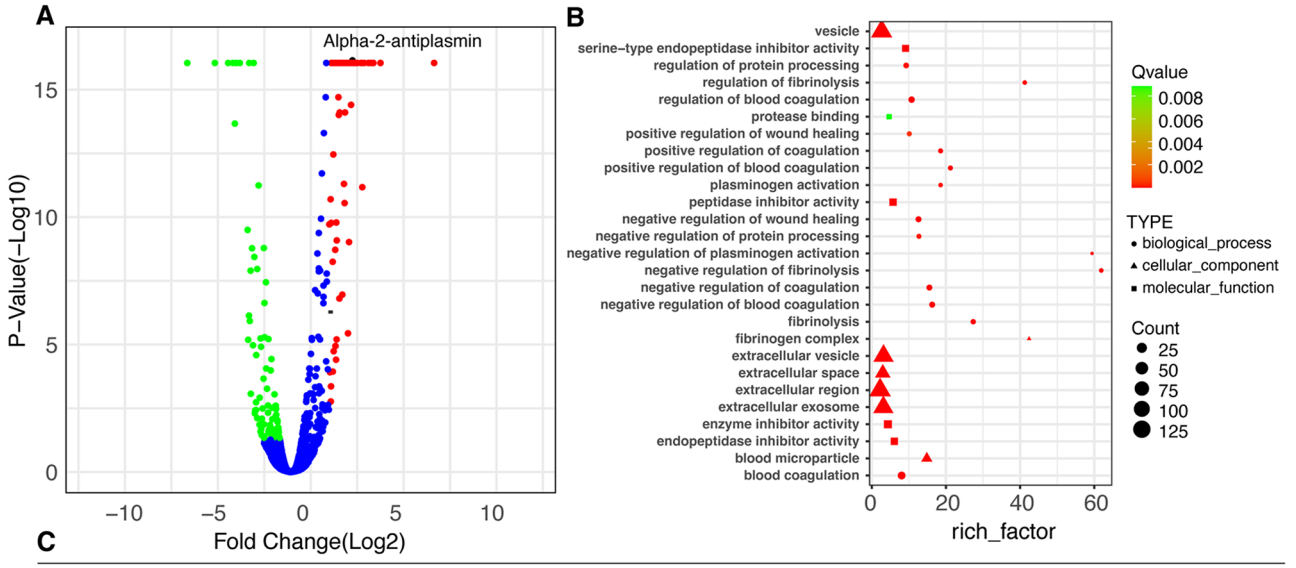

C

Upregulated Proteins			Downregulated Proteins		
Protein ID	**Protein Name**	**Log2(Fold Change)**	**Protein ID**	**Protein Name**	**Log2(Fold Change)**
Q61838	Alpha-2-macroglobulin	6.643	Q3TF41	Nucleosome assembly protein 1-like 1	-1.220
P23953	Carboxylesterase 1C	3.374	P35441	Thrombospondin-1	-1.718
P28665	Murinoglobulin-1	3.259	P12388	Plasminogen activator inhibitor 2	-1.796
Q91X72	Hemopexin	3.105	P58252	Elongation factor 2	-1.852
Q00623	Apolipoprotein A-I	2.877	O08675	Proteinase-activated receptor 3	-1.868
A0A0R4J0I1	Serine protease inhibitor A3K	2.470	P50228	C-X-C motif chemokine 5	-2.070
P06728	Apolipoprotein A-IV	2.469	Q921H8	3-ketoacyl-CoA thiolase A	-2.152
D3YTY9	Kininogen-1	2.364	O70591	Prefoldin subunit 2	-2.192
O89020	Afamin	2.289	Q06770	Corticosteroid-binding globulin	-2.411
P01027	Complement C3	2.250	P55144	Tyrosine-protein kinase receptor TYRO3	-2.540
Q61247	Alpha-2-antiplasmin	2.248	Q921J2	GTP-binding protein RhebA	-2.515
Q921I1	Serotransferrin	2.114	P14106	Complement C1q subcomponent subunit B	-2.878
P07724	Serum albumin	1.945			
B8JJM5	Complement factor B	1.827	P70297	Signal transducing adapter molecule 1	-3.224
E9Q810	Complement factor H	1.735	Q7TT36	Adhesion G protein-coupled receptor A3	-3.238
G3X977	Inter-alpha-trypsin inhibitor	1.690	Q62165	Dystroglycan	-3.308
A0A087WSN6	Fibronectin	1.660	P62806	Histone H4	-3.816
P20918	Plasminogen	1.626	Q9DC70	NADH dehydrogenase	-3.396
P32261	Antithrombin-III	1.505	Q64442	Sorbitol dehydrogenase	-4.012
P01898	H-2 class I histocompatibility antigen	1.492	Q5NCX5	Neuralized-like protein 4	-5.158
			P43274	Histone H1.4	-6.648

Figure 4. Platelet proteomics analysis identified differentially expressed proteins. (A) The analysis of the platelet proteomics from the OC-VTE and control groups revealed differentially expressed proteins, including upregulated and downregulated proteins. The black spot indicated alpha-2-antiplasmin. (B) Gene Ontology analysis suggested that these differentially expressed proteins are mostly enriched in the biological process of negative regulation of fibrinolysis as well as the cellular component of the fibrinogen complex. (C) Top 20 upregulated and 20 downregulated proteins are shown.

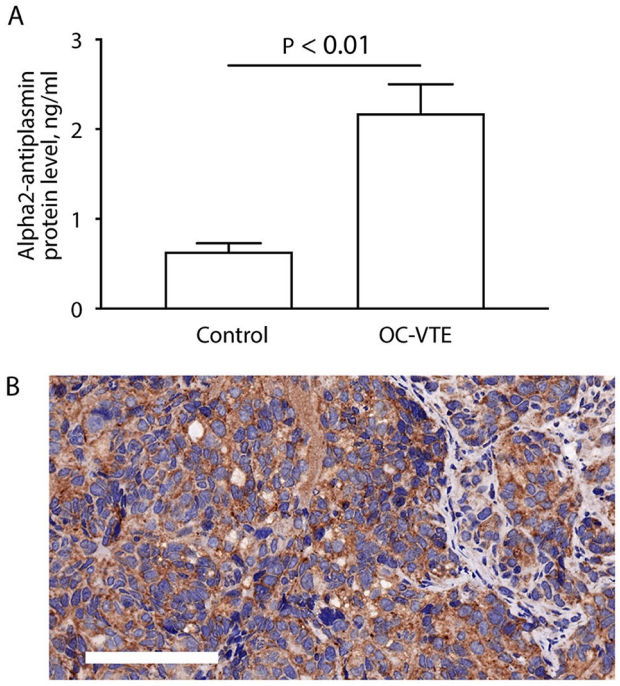

Figure 5. Validation of platelet proteomic analysis identified differential protein alpha-2-antiplasmin. (A) ELISA was performed to validate the protein level of alpha-2-antiplasmin in the mouse plasma. The data were shown as mean ± standard deviation and were analyzed using Student's *t* test. (B) Immunohistochemistry was applied to detect the expression of alpha-2-antiplasmin in the tumor section from the OC-VTE group. Scale bar, 100 µm.

of which play key roles in the process of thrombosis (Figure 4(B)). Importantly, one of the upregulated proteins identified in our platelet proteomics was alpha-2-antiplasmin (Figure 4(A), black spot), which has been reported to be essential for stasis-induced thrombus development.[23]

In order to further confirm the results from the mass spectrometry experiment, we performed ELISA analysis to characterize the protein expression level of alpha-2-antiplasmin using the plasma from the control and OC-VTE groups. The data showed that alpha-2-antiplasmin protein levels were increased in the plasma of the mouse from the OC-VTE group compared with the control group (Figure 5(A)). We further confirmed the high expression levels of alpha-2-antiplasmin in the tumor section of the OC-VTE group mouse (Figure 5(B)). Together with its discovery as a secreted protein[24] and the role it plays in accelerating thrombus formation,[23] our results suggest that alpha-2-antiplasmin might be involved in ovarian cancer–induced VTE.

Discussion

The establishment of cancer-associated VTE models is important since the risk factors of VTE formation differ between cancer types.[20] Here, we generated a mouse model of OC-VTE. Further analysis using this model revealed that negative fibrinolysis and fibrinogen complex regulation might participate in the formation of OC-VTE.

Animal VTE models are the key to unraveling the underlying mechanisms of how cancer-associated VTE initiates and develops. Locally induced hypercoagulability in the rodent VTE model is triggered by surface presoaking using ferric chloride, which induces oxidative damage to the vessel wall.[16,25–27] This model generates acute VTE and, therefore, cannot mimic the condition of chronic VTE, such as cancer-associated VTE.[28] The IVC stasis model, in which the IVC of the animal is completely obstructed, has been used to examine the detailed mechanisms of thrombi formation.[29–31] The defect of this complete IVC stasis is that this strategy of VTE modeling induces endothelial injury.[28] Thus, it is not ideal for mimicking cancer-induced thrombosis. However, in IVC stenosis models, the IVC lumen is reduced but not completely blocked, increasing the risk of developing VTE but with minimal endothelial damage.[18,32] IVC stenosis models have been used to study VTE initiation mediated by platelets and coagulation factors.[13] Taken together, the strategy of IVC stenosis is suitable for generating VTE models to unravel the risk factors of VTE formation in the context of cancer.

Ovarian cancer carries a high risk of VTE and it is urgent to establish an animal model to study the underlying mechanisms of OC-VTE. After optimizing surgical practice, half of the mice from the OC-VTE group developed VTE, while none of the mice from the control group developed VTE (Table 1). To our knowledge, this is the first to report an OC-VTE animal model. However, one limitation of our work is that we did not use various ovarian cancer cell lines and patient-derived xenografts to induce OC-VTE in parallel. Therefore, further work is needed to confirm the robustness of ovarian cancer–induced VTE in this mouse model in the future. Nevertheless, this study provides a feasible tool to investigate the underlying mechanisms of VTE formation in ovarian cancer.

Cancer-associated VTE is associated with the secretion of coagulation factors by cancer cells, including TF, podoplanin, plasminogen activation inhibitor-1, and cancer procoagulant. These factors are involved in cancer-associated VTE formation. In addition, a chronic low-grade inflammatory state, which is due to inflammatory cytokine secretion by the cancer cells, leads to a pro-activation state of the platelets to promote cancer-associated VTE development. Patients with ovarian cancer with high platelet levels and high D-dimer levels are at high risk of postoperative VTE. However, previous studies have not identified the exact molecules that modulate platelet function in the formation of OC-VTE.

In order to reveal the underlying mechanism of how platelets mediate OC-VTE, we performed a proteomics analysis using the platelets of the mice from the OC-VTE and control groups. This identified the differentially expressed proteins between the two groups. These differentially expressed proteins are involved in the negative regulation of fibrinolysis and the cellular component of the fibrinogen complex, which play key roles in the process of thrombosis. Specifically, alpha-2-antiplasmin was upregulated in the platelets of the OC-VTE group, which has been reported to promote thrombus formation. Alpha-2-antiplasmin is a coagulation-promoting factor that inhibits the fibrinolytic system and enhances the formation of microthrombi and is associated with poor outcomes of cardiovascular diseases. Therefore, we speculate that alpha-2-antiplasmin participates in OC-VTE. The

emerging question is how the level of alpha-2-antiplasmin is regulated in platelets. Our study reveals that alpha-2-antiplasmin is highly expressed in ovarian cancer tumor sections. We then speculate that the higher expression level of alpha-2-antiplasmin in the mouse from the OC-VTE group might be due to the protein secretion from the ovarian cancer cells as alpha-2-antiplasmin is a secretory protein.[24] However, this should be validated in the future, using *in vitro* experimental approaches and clinical samples. Another limitation of this study is the absence of detailed characterization of platelet activity in the context of OC-VTE. It can be further examined using the platelets from our OC-VTE model and ovarian cancer patients with VTE in the future.

Taken together, we have generated an OC-VTE mouse model, which represents a future research direction that warrants investigation of the underlying mechanisms of how ovarian cancer promotes VTE formation. Our study likely lays the foundation for such inquiries.

AUTHORS' CONTRIBUTIONS

RZ and YZ supervised the project. SM and SY conducted experiments. SM, SY, YZ, and RZ wrote the manuscript.

DECLARATION OF CONFLICTING INTERESTS

The author(s) declared no potential conflicts of interest with respect to the research, authorship, and/or publication of this article.

FUNDING

The author(s) disclosed receipt of the following financial support for the research, authorship, and/or publication of this article: This work was supported by the Science and Technology Commission of Shanghai Municipality (18140902300) to RZ.

ORCID ID

Sining Ma https://orcid.org/0000-0002-9895-5168

REFERENCES

1. Kisseleva T, Brenner D. Molecular and cellular mechanisms of liver fibrosis and its regression. *Nat Rev Gastroenterol Hepatol* 2021;**18**:151–66
2. Farge D, Frere C, Connors JM, Ay C, Khorana AA, Munoz A, Brenner B, Kakkar A, Rafii H, Solymoss S, Brilhante D, Monreal M, Bounameaux H, Pabinger I, Douketis J, International Initiative on Thrombosis and Cancer (ITAC) Advisory Panel. 2019 international clinical practice guidelines for the treatment and prophylaxis of venous thromboembolism in patients with cancer. *Lancet Oncol* 2019;**20**:e566–81
3. Watson HG, Keeling DM, Laffan M, Tait RC, Makris M, British Committee for Standards in Haematology. Guideline on aspects of cancer-related venous thrombosis. *Br J Haematol* 2015;**170**:640–8
4. Key NS, Khorana AA, Kuderer NM, Bohlke K, Lee AYY, Arcelus JI, Wong SL, Balaban EP, Flowers CR, Francis CW, Gates LE, Kakkar AK, Levine MN, Liebman HA, Tempero MA, Lyman GH, Falanga A. Venous thromboembolism prophylaxis and treatment in patients with cancer: ASCO clinical practice guideline update. *J Clin Oncol* 2020;**38**:496–520
5. Sorensen HT, Mellemkjaer L, Olsen JH, Baron JA. Prognosis of cancers associated with venous thromboembolism. *N Engl J Med* 2000;**343**:1846–50
6. Khorana AA, Francis CW, Culakova E, Kuderer NM, Lyman GH. Thromboembolism is a leading cause of death in cancer patients receiving outpatient chemotherapy. *J Thromb Haemost* 2007;**5**:632–4
7. Farge D, Bounameaux H, Brenner B, Cajfinger F, Debourdeau P, Khorana AA, Pabinger I, Solymoss S, Douketis J, Kakkar A. International clinical practice guidelines including guidance for direct oral anticoagulants in the treatment and prophylaxis of venous thromboembolism in patients with cancer. *Lancet Oncol* 2016;**17**:e452–66
8. Lyman GH, Culakova E, Poniewierski MS, Kuderer NM. Morbidity, mortality and costs associated with venous thromboembolism in hospitalized patients with cancer. *Thromb Res* 2018;**164**:S112–8
9. Strom Kahr H, Christiansen OB, Juul Riddersholm S, Gade IL, Torp-Pedersen C, Knudsen A, Thorlacius-Ussing O. The timing of venous thromboembolism in ovarian cancer patients: a nationwide Danish cohort study. *J Thromb Haemost* 2021;**19**:992–1000
10. Satoh T, Oki A, Uno K, Sakurai M, Ochi H, Okada S, Minami R, Matsumoto K, Tanaka YO, Tsunoda H, Homma S, Yoshikawa H. High incidence of silent venous thromboembolism before treatment in ovarian cancer. *Br J Cancer* 2007;**97**:1053–7
11. Khan F, Tritschler T, Kahn SR, Rodger MA. Venous thromboembolism. *Lancet* 2021;**398**:64–77
12. Falati S, Liu Q, Gross P, Merrill-Skoloff G, Chou J, Vandendries E, Celi A, Croce K, Furie BC, Furie B. Accumulation of tissue factor into developing thrombi in vivo is dependent upon microparticle P-selectin glycoprotein ligand 1 and platelet P-selectin. *J Exp Med* 2003;**197**:1585–98
13. Brill A, Fuchs TA, Chauhan AK, Yang JJ, De Meyer SF, Kollnberger M, Wakefield TW, Lämmle B, Massberg S, Wagner DD. von Willebrand factor-mediated platelet adhesion is critical for deep vein thrombosis in mouse models. *Blood* 2011;**117**:1400–7
14. Diaz JA, Obi AT, Myers DD Jr, Wrobleski SK, Henke PK, Mackman N, Wakefield TW. Critical review of mouse models of venous thrombosis. *Arterioscler Thromb Vasc Biol* 2012;**32**:556–62
15. Wang X, Smith PL, Hsu MY, Tamasi JA, Bird E, Schumacher WA. Deficiency in thrombin-activatable fibrinolysis inhibitor (TAFI) protected mice from ferric chloride-induced vena cava thrombosis. *J Thromb Thrombolysis* 2007;**23**:41–9
16. Herbert JM, Bernat A, Maffrand JP. Importance of platelets in experimental venous thrombosis in the rat. *Blood* 1992;**80**:2281–6
17. Myers D Jr, Farris D, Hawley A, Wrobleski S, Chapman A, Stoolman L, Knibbs R, Strieter R, Wakefield T. Selectins influence thrombosis in a mouse model of experimental deep venous thrombosis. *J Surg Res* 2002;**108**:212–21
18. von Bruhl ML, Stark K, Steinhart A, Chandraratne S, Konrad I, Lorenz M, Khandoga A, Tirniceriu A, Coletti R, Köllnberger M, Byrne RA, Laitinen I, Walch A, Brill A, Pfeiler S, Manukyan D, Braun S, Lange P, Riegger J, Ware J, Eckart A, Haidari S, Rudelius M, Schulz C, Echtler K, Brinkmann V, Schwaiger M, Preissner KT, Wagner DD, Mackman N, Engelmann B, Massberg S. Monocytes, neutrophils, and platelets cooperate to initiate and propagate venous thrombosis in mice in vivo. *J Exp Med* 2012;**209**:819–35
19. Diaz JA, Saha P, Cooley B, Palmer OR, Grover SP, Mackman N, Wakefield TW, Henke PK, Smith A, Lal BK. Choosing a mouse model of venous thrombosis: a consensus assessment of utility and application. *J Thromb Haemost* 2019;**17**:699–707
20. Hisada Y, Mackman N. Mouse models of cancer-associated thrombosis. *Thromb Res* 2018;**164**:S48–53
21. Timp JF, Braekkan SK, Versteeg HH, Cannegieter SC. Epidemiology of cancer-associated venous thrombosis. *Blood* 2013;**122**:1712–23
22. Wang JG, Geddings JE, Aleman MM, Cardenas JC, Chantrathammachart P, Williams JC, Kirchhofer D, Bogdanov VY, Bach RR, Rak J, Church FC, Wolberg AS, Pawlinski R, Key NS, Yeh JJ, Mackman N. Tumor-derived tissue factor activates coagulation and enhances thrombosis in a mouse xenograft model of human pancreatic cancer. *Blood* 2012;**119**:5543–52
23. Singh S, Houng AK, Reed GL. Venous stasis-induced fibrinolysis prevents thrombosis in mice: role of alpha2-antiplasmin. *Blood* 2019;**134**:970–8
24. Abdul S, Leebeek FW, Rijken DC, Uitte de Willige S. Natural heterogeneity of alpha2-antiplasmin: functional and clinical consequences. *Blood* 2016;**127**:538–45
25. Vogel GM, Meuleman DG, Bourgondien FG, Hobbelen PM. Comparison of two experimental thrombosis models in rats effects of four glycosaminoglycans. *Thromb Res* 1989;**54**:399–410

26. Wessler S. Thrombosis in the presence of vascular stasis. *Am J Med* 1962;**33**:648–66
27. Wessler S, Gitel SN, Bank H, Martinowitz U, Stephenson RC. An assay of the antithrombotic action of warfarin: its correlation with the inhibition of stasis thrombosis in rabbits. *Thromb Haemost* 1979;**40**:486–98
28. Albadawi H, Witting AA, Pershad Y, Wallace A, Fleck AR, Hoang P, Khademhosseini A, Oklu R. Animal models of venous thrombosis. *Cardiovasc Diagn Ther* 2017;**7**:S197–206
29. Bernat A, Vallee E, Maffrand JP, Roncucci R. Antithrombotic effect of ticlopidine in a platelet-independent model of venous thrombosis. *Thromb Res* 1985;**37**:279–85
30. Doutremepuich C, Gestreau JL, Maury MO, Quilichini R, Boisseau MR, Toulemonde F, Vairel E. Experimental venous thrombosis in rats treated with heparin and a low molecular weight heparin fraction. *Haemostasis* 1983;**13**:109–12
31. Thomas DP, Merton RE, Hockley DJ. The effect of stasis on the venous endothelium: an ultrastructural study. *Br J Haematol* 1983;**55**:113–22
32. Brill A, Fuchs TA, Savchenko AS, Thomas GM, Martinod K, De Meyer SF, Bhandari AA, Wagner DD. Neutrophil extracellular traps promote deep vein thrombosis in mice. *J Thromb Haemost* 2012;**10**:136–44

(Received February 23, 2022, Accepted June 20, 2022)